

Enhanced image reconstruction of electrical impedance tomography using simultaneous algebraic reconstruction technique and K-means clustering

Arfan Eko Fahrudin^{1,2}, Endarko¹, Khusnul Ain³, Agus Rubiyanto¹

¹Laboratory of Medical Physics and Biophysics, Institut Teknologi Sepuluh Nopember, East Java, Indonesia

²Physics Study Program, Universitas Lambung Mangkurat, Banjarbaru, Indonesia

³Department of Physics, Universitas Airlangga, Surabaya, Indonesia

Article Info

Article history:

Received Nov 21, 2022

Revised Jan 5, 2023

Accepted Feb 4, 2023

Keywords:

Butterworth low-pass filter
Electrical impedance tomography
Image reconstruction
K-means clustering
Simultaneous algebraic reconstruction technique algorithm

ABSTRACT

Electrical impedance tomography (EIT), as a non-ionizing tomography method, has been widely used in various fields of application, such as engineering and medical fields. This study applies an iterative process to reconstruct EIT images using the simultaneous algebraic reconstruction technique (SART) algorithm combined with K-means clustering. The reconstruction started with defining the finite element method (FEM) model and filtering the measurement data with a Butterworth low-pass filter. The next step is solving the inverse problem in the EIT case with the SART algorithm. The results of the SART algorithm approach were classified using the K-means clustering and thresholding. The reconstruction results were evaluated with the peak signal noise ratio (PSNR), structural similarity indices (SSIM), and normalized root mean square error (NRMSE). They were compared with the one-step gauss-newton (GN) and total variation regularization based on iteratively reweighted least-squares (TV-IRLS) methods. The evaluation shows that the average PSNR and SSIM of the proposed reconstruction method are the highest of the other methods, each being 24.24 and 0.94; meanwhile, the average NRMSE value is the lowest, which is 0.04. The performance evaluation also shows that the proposed method is faster than the other methods.

This is an open access article under the [CC BY-SA](https://creativecommons.org/licenses/by-sa/4.0/) license.



Corresponding Author:

Endarko

Laboratory of Medical Physics and Biophysics, Institut Teknologi Sepuluh Nopember

Kampus ITS-Sukolilo Surabaya, Surabaya-60111, East Java, Indonesia

Email: endarko@physics.its.ac.id

1. INTRODUCTION

In recent years, research on electrical impedance tomography (EIT) has overgrown with applications in various fields, such as engineering (materials, civil, and chemical) and medical imaging. Usefulness in engineering, such as [1] for visualizing the distribution of conductivity on carbon nanotube (CNT) composite layers, for analysis of building moisture conditions [2], and for imaging of chemical engineering process [3]. Meanwhile, some examples of the application of EIT in the medical field include the imaging of stroke patients [4], imaging of breast cancer detection [5], imaging of lung ventilation [6], and cardiopulmonary monitoring [7]. The advantages of EIT being chosen for some of these applications are that EIT is available in a low-cost system, non-ionizing, and non-invasive to the object being measured or observed [8].

Research on EIT development generally has two topics: hardware and software development. Research on hardware development, among others, focuses on the design and fabrication of constant current

sources [9], [10], and there is also a focus on the design and fabrication of the overall EIT system, both based on microcontrollers [11], microprocessors [12], [13] and also field programmable gate arrays (FPGA) [14]. Research in software development for EIT includes the development of regularization-based reconstruction algorithms [15]–[18], with the iterative method [19], [20] simulated annealing [21], [22], genetic algorithms [23] and deep learning [24], [25]. In addition to developing reconstruction algorithms, there are studies on using digital filters [26] and clustering to support the EIT image reconstruction algorithm [27].

The iterative method is one of the reliable approaches for image reconstruction, such as X-ray and impedance tomography. Research that uses iterative methods on EIT reconstruction, among others, using optimal current patterns to distinguish the actual conductivity from the estimated conductivity between each iteration of the block Kaczmarz algorithm to solve the inverse problem [28] and a modified Landweber iterative algorithm that is based on an updated sensitivity matrix [29]. The structured sparse representation is added to the iterative process of the Symkaczmarz algorithm for EIT image reconstruction to enhance the quality of the reconstruction presented in [30]. In another research, a linear back-projection (ILBP) is suggested to reduce the presence of artifacts around objects and increase the accuracy of object position and shape [20]. In [31], EIT reconstruction was conducted based on homotopy perturbation iteration (HPI), which accelerated with Nesterov's strategy. While those that use iterative methods on X-ray imaging are modifications of the simultaneous algebraic reconstruction technique (SART) algorithm with total variation regularization [32], modification of the SART algorithm with one step late (OSL) technique [33], modified SART based on the Perona-Malik (PM) model [34], and modified SART algorithm with fast total variation for positron-emission tomography (PET) imaging [35]. Meanwhile, in another study SART algorithm was applied to ionospheric tomography [36] and microwave imaging [37].

Based on the advantages of these iterative methods, especially the SART algorithm, this study uses the iterative SART method as the EIT reconstruction algorithm. The SART algorithm is then combined with the K-means clustering algorithm and followed by thresholding to improve the quality of the reconstructed image output. The study was conducted by simulation and experiment using a two-dimensional (2D) cylindrical phantom with an anomaly object as the output of the reconstructed image.

2. METHOD

In this study, the EIT image reconstruction process was carried out by simulation and experiment implemented with electrical impedance and diffuse optical reconstruction software (EIDORS) [38] and Air Tool [39] in MATLAB. The simulation process started by creating the phantom model. The phantom or object measured for the simulation was a 2D cylinder with 16 electrodes. The finite element method (FEM) model of the phantom was created with Netgen within EIDORS. Figure 1 shows an example of a phantom with an anomaly, Figure 1(a) shows it with the *show_fem* function, and Figure 1(b) displays it in the *show_slices* function of EIDORS. The anomaly given to the phantom is in a circle and rectangle form in the simulation, as shown in Figure 2. The background conductivity of the phantom is 1 S/m, and the anomalous object has a conductivity of 2.2 and 0.1 S/m. So that the EIT simulation is similar to the actual conditions, in the simulation process, noise is given to the measurement data with a gaussian noise of 40 dB signal to noise ratio (SNR). The measurement data of simulation obtained from the electrodes when current is driving into the phantom. In The EIODRS, type of current driving and voltage measurement method must be set first. Current driving and voltage measurements are performed using the commonly used adjacent method [40]. The principle of the adjacent method is illustrated in Figure 3, an example of the initial step of the adjacent method is shown in Figure 3(a), and the following step is in Figure 3(b).

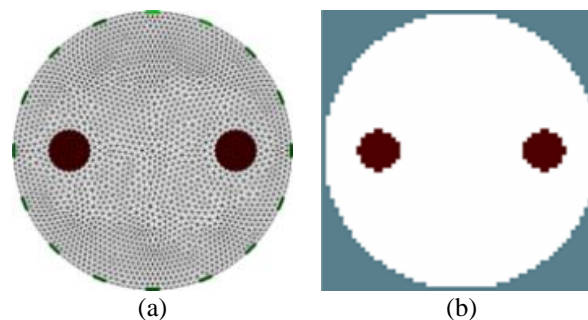


Figure 1. Phantom with an anomaly (a) displayed with *show_fem* and (b) displayed with *show_slices*

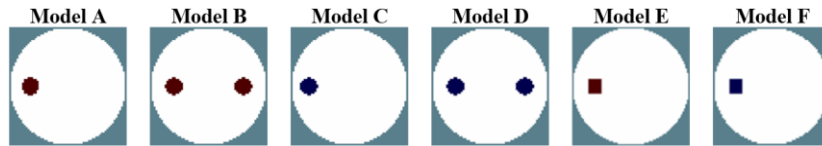


Figure 2. Anomalous models (conductivity of models A, B, and E is 2.2 S/m, models C, D, and F is 0.1 S/m)

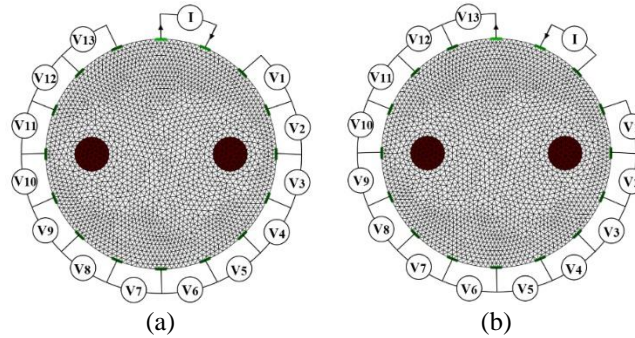


Figure 3. Illustration adjacent method in the current (I) driving and voltage (V) measurement: (a) initial step and (b) second step

The next stage of simulation is the reconstruction process and evaluation with steps as illustrated in Figure 4. The reconstruction process started with defining of FEM model for reconstruction. This study used a standard model of FEM on EIDORS with mesh elements of 6,400, as shown in Figure 5. Before the data of EIT measurement is processed with a reconstruction algorithm, a filtering process is carried out with a first-order Butterworth low pass filter to reduce noise from the measurement data. The filtered measurement data is the difference in the voltage read on the phantom when there is an anomaly (inhomogeneous) and no anomaly (homogeneous). The low pass filter has a normalized cut-off frequency of 0.45.

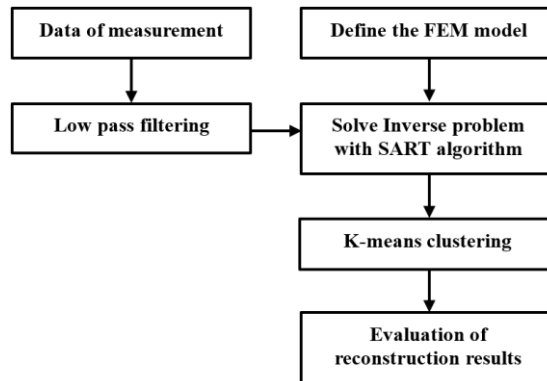


Figure 4. Steps of the reconstruction process and evaluation

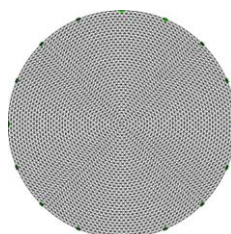


Figure 5. FEM model of the image reconstruction

In the inverse problem for EIT, by ignoring the high-order terms, the linear approximation of the EIT model can be expressed in (1) [41],

$$\delta U = J\delta\sigma \quad (1)$$

where $\delta U \in R^{m \times 1}$ is the number m measurement data, $\delta\sigma \in R^{n \times 1}$ is the reconstructed image with the number of n pixels, and $J \in R^{m \times n}$ is the reconstruction matrix or sensitivity matrix with dimensions $m \times n$, representing the partial derivative of the voltage associated with conductivity. To solve the linear system problem of EIT, the SART algorithm, as one of the iterative methods, is used to solve the inversion problem for image reconstruction. The (1) can be restated as $b = ax$, where $b = \delta U$, $a = J$, and $x = \delta\sigma$, so that the solution to the linear equation with the SART algorithm becomes (2), with λ (lambda) is a relaxation parameter satisfying $0 < \lambda < 2$, and as default in Air Tool λ is set to 1. The application of the SART algorithm begins by providing an initial value of x_0 (usually $x_0=0$) as input and then iterates until the convergent condition is met. The iteration process of the SART algorithm is expressed in (2) [35].

$$x_j^{k+1} = x_j^k + \frac{\lambda}{\sum_{i=1}^M a_{i,j}} \sum_{j=1}^M a_{i,j} \frac{b_i - \sum_{l=1}^M a_{i,l} x_l^k}{\sum_{l=1}^M a_{i,l}} \quad (2)$$

The output of the SART algorithm is then classified using the K-means algorithm, specifically the K-means++ algorithm, an improved version of K-means. An explanation of the K-means++ clustering algorithm can be seen in [42]. The SART algorithm output in a $6,400 \times 1$ matrix that is classified into six classes, and the centroids of these classes are sorted ascending. The class with the lowest centroid shows the smallest conductivity; otherwise, the class with the largest centroid has the highest conductivity. After the classification, the thresholding process is carried out to display only anomalous objects in the reconstructed image. For anomalies whose conductivity is higher than the background, the thresholding process is carried out with the maximum value of the matrix, which belongs to the largest centroid class, so that the maximum value is the object and the background is the minimum value; for smaller conductivities, the opposite applies. The next step is to reconstruct the image by applying the results of classification and thresholding into the mesh of the FEM model used.

Furthermore, the reconstruction results from the proposed method are compared with one-step gauss-newton (GN) [43] and total variation regularization based on iteratively reweighted least-squares (TV-IRLS) [17]. The implementation of both methods (one-step (GN) and TV-IRLS) is performed with the inbuilt algorithm of EIDORS. The optimal reconstruction result of these compared methods is achieved by determining the hyperparameter or regularization parameter with the L-curve method. The parameters used to evaluate the reconstruction results are peak signal noise ratio (PSNR), structural similarity indices (SSIM), and normalized root mean square error (NRMSE). PSNR is used as an objective measure of image quality which is expressed by (3) [44],

$$PSNR = 10 \log_{10} \left(\frac{peakval^2}{MSE} \right) \quad (3)$$

where $peakval$ is the maximum pixel value of the reference image (ground truth), and MSE is the mean square error between the reconstructed image and the reference image. SSIM is a measure of image quality that represents the similarity of two images, where SSIM is obtained by calculating the components of luminance (I), contrast (c), and correlation coefficient (s) so that SSIM is defined by [45]:

$$SSIM(x, y) = [I(x, y)]^\alpha [c(x, y)]^\beta [s(x, y)]^\gamma$$

with

$$I(x, y) = \frac{2\mu_x\mu_y + C_1}{\mu_x^2 + \mu_y^2 + C_1},$$

$$c(x, y) = \frac{2\sigma_x\sigma_y + C_2}{\sigma_x^2 + \sigma_y^2 + C_2},$$

$$s(x, y) = \frac{\sigma_{xy} + C_3}{\sigma_x\sigma_y + C_3}$$

where $\mu_x, \mu_y, \sigma_x, \sigma_y$ and σ_{xy} are the local mean, standard deviation, and cross-covariance of the image. Meanwhile, C_1, C_2 and C_3 are constant, with $C_1 = (K_1L)^2, C_2 = (K_2L)^2$ where $K_1 \ll 1, K_2 \ll 1$, each is a small constant, and L is the dynamic range of the pixel values. To simplify the SSIM formula, the value of $\alpha=\beta=\gamma=1$ and $C_3=C_2/2$ so that the SSIM formula becomes:

$$SSIM(x, y) = \frac{(2\mu_x\mu_y+C_1)(2\sigma_{xy}+C_2)}{(\mu_x^2+\mu_y^2+C_1)(\sigma_x^2+\sigma_y^2+C_2)} \quad (4)$$

Another metric used to evaluate reconstruction results is NRMSE which is defined as (5) [46],

$$NRMSE = \sqrt{\frac{\sum(I_{ref}(r) - I(r))^2}{\sum(I_{ref}(r))^2}} \quad (5)$$

where $I_{ref}(r)$ denotes reference image and $I(r)$ is a reconstructed image.

Experimental data on EIT was obtained from a microcontroller-based EIT hardware system with a design as shown in Figure 6. The measuring object or phantom was a cylinder with a diameter of 14 cm and 16 electrodes with dimensions of $1 \times 2 \text{ cm}^2$. The cylinder is then filled with saline water with a conductivity of $912 \mu\text{S/cm}$, as high as 1.5 cm. The anomalous objects are a brass cylinder rod with a diameter of 2.2 cm, a copper block with a side of 2.5 cm, a painted wooden cylinder with a diameter of 2.7 cm, and a wooden cube with a side of 2.7 cm. Reconstructing the experimental data has the same steps as reconstruction through simulation. The reconstruction results are then evaluated qualitatively by comparing the reconstructed image to the actual condition of the object.

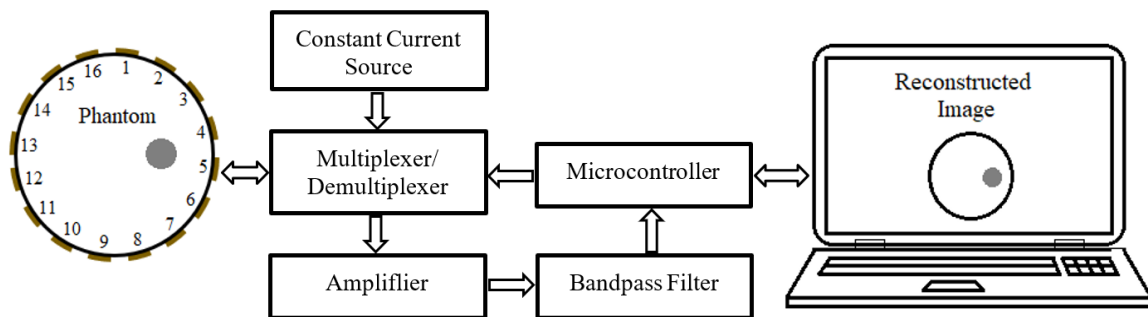


Figure 6. EIT hardware design diagram

3. RESULTS AND DISCUSSION

In this research, an iterative method with the SART algorithm for EIT image reconstruction is used to detect anomalous objects in cylindrical phantom, which have higher and lower conductivity than background conductivity. The results of applying the low pass filter with the SART algorithm are shown in Figure 7. From the figure, it can be seen that there is a reduction in noise from the reconstructed image. This noise reduction can be seen from the increase in the PSNR value. In addition, visually, it can be seen that the anomalies in the reconstructed image are more similar in shape to the original image.

A comparison of the reconstruction results of the proposed method with one-step GN and TV-IRLS from the simulation is shown in Figure 7. Evaluation results with PSNR, SSIM, and NRMSE reconstruction parameters from all methods indicate that the reconstructed image with the proposed method results in the more optimal result of the image. This optimal result is shown from the PSNR and SSIM values, which increase after clustering and thresholding; otherwise, the values of NRMSE decrease. The average of PSNR and SSIM values of the proposed method are 24.24 and 0.94, respectively, whereas the highest value of PSNR and SSIM from other methods, meanwhile the average of NRMSE is 0.04, which is the lowest value from other methods. Comparison of PSNR, SSIM, and NRMSE values from each model for different methods are also shown in Figures 8 to 10, it is demonstrated that the proposed method has the highest PSNR and SSIM values and the lowest value of NRMSE. The optimal value of this parameter is due to the image's background noise, which can be optimally reduced so that the reconstruction results are close to the ground truth.

In addition to indicating the reconstructed image quality, the NRMSE value is also related to the reconstructed image accuracy. The smaller the NRMSE value, the more accurate the resulting reconstructed image will be. This accuracy can be seen from the shape and position of the reconstructed image. Based on

the reconstructed image, as shown in Figure 7, the sixth column, it can be seen that the smaller the RMSE value, the shape and position of the reconstructed image are more accurate and closer to the reference image, and vice versa.

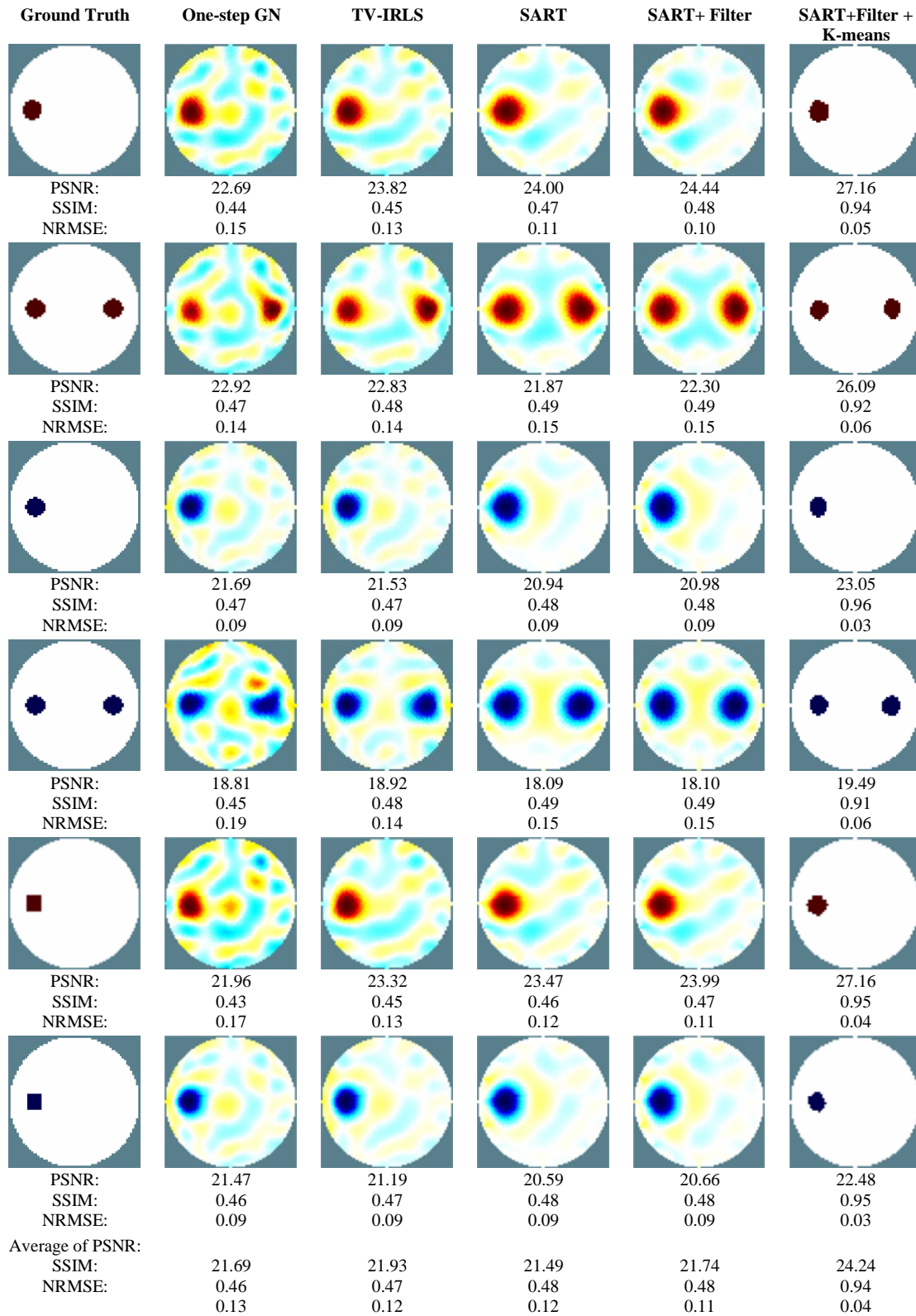


Figure 7. Reconstruction results through simulation

The results of the reconstruction by experiment are shown in Figure 11. Based on the experimental results, it can be seen that the results of the reconstruction with the SART+filter method obtained results that were similar to the results of the reconstruction with a simulation, where the resulting image compared with the actual conditions obtained similar results, both from the shape and position. The reconstructed image shows better results than the one-step GN and TV-IRLS methods. Likewise, the reconstruction results obtained by combining the SART algorithm with K-means clustering show significantly better results than the reconstruction results using other methods, where the reconstruction results clearly show the anomalous objects.

Apart from being observed from the reconstruction results, the proposed method's performance is also tested based on the computation time. Table 1 shows the computation time of the three methods used during the experiment, which were run on a laptop equipped with an Intel(R) Core(TM) i7-6600U CPU and 8 GB of RAM. The Table 1 shows that the proposed method has a low-cost computation time compared to other methods, proving that the algorithm is efficient for solving EIT image reconstruction problems.

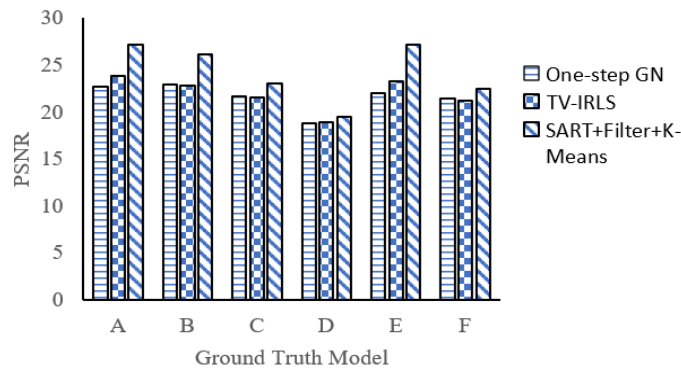


Figure 8. Comparison of PSNR values for different methods

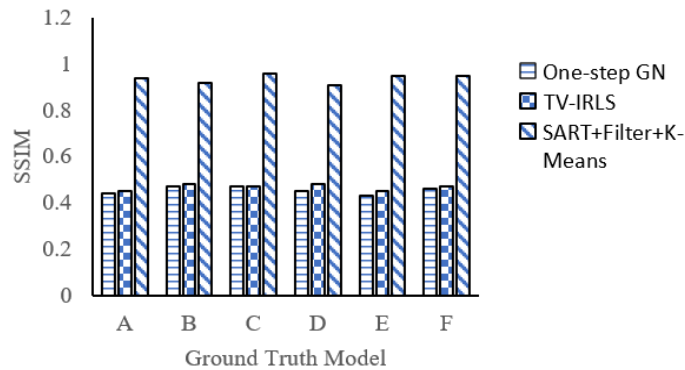


Figure 9. Comparison of SSIM values for different methods

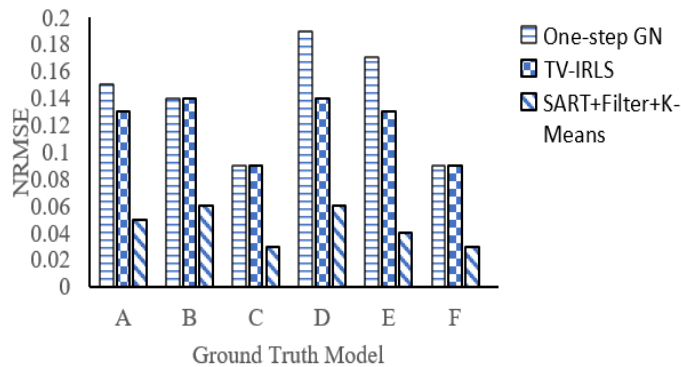


Figure 10. Comparison of NRMSE values for different methods

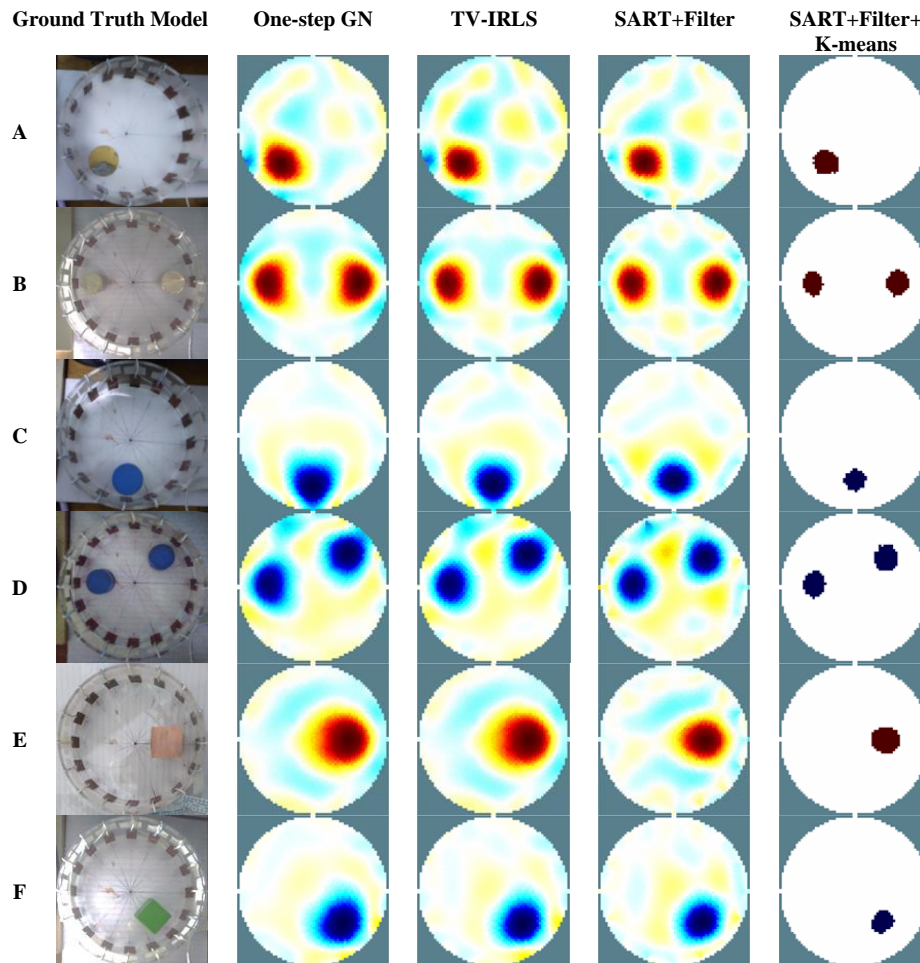


Figure 11. Reconstruction results through experiment

Table 1. Time of computation of each method based on the experiment

Method	Reconstruction time (s)					
	Model A	Model B	Model C	Model D	Model E	Model F
One step GN	4.32	4.38	4.36	4.36	4.18	4.39
TV-IRLS	21.86	23.59	22.02	21.98	24.44	21.87
SART+Filter+K-means	1.80	1.76	1.79	1.86	1.80	1.78

4. CONCLUSION

The reconstructed image from the EIT with the SART algorithm combined with K-means clustering demonstrated provides a reasonably optimal image of the reconstruction result. This optimal result is shown from the evaluation results of the reconstructed image through simulation, in which quantitatively obtained average PSNR and SSIM are the highest compared to other methods; the values are 24.24 and 0.94, respectively, and the lowest NRMSE with the value 0.04. Meanwhile, referring to the experiment, qualitatively, the reconstructed image obtained is similar to the image reconstruction using simulation, and the results are close to the actual conditions of the reconstructed object. In the performance evaluation of the experiment compared with one-step GN and TV-IRLS, the proposed method is faster than the other methods.

ACKNOWLEDGEMENTS

The author would like to thank the Ministry of Education, Culture, Research, and Technology, which has provided Domestic Postgraduate Education Scholarships (BPPDN) and gratefully acknowledge the financial support from the Institut Teknologi Sepuluh Nopember with scheme collaboration research Number: 1233/PKS/ITS/2021.





REFERENCES

- [1] T.-C. Hou, K. J. Loh, and J. P. Lynch, "Spatial conductivity mapping of carbon nanotube composite thin films by electrical impedance tomography for sensing applications," *Nanotechnology*, vol. 18, no. 31, Aug. 2007, doi: 10.1088/0957-4484/18/31/315501.
- [2] T. Rymarczyk, J. Sikora, and P. Tchórzewski, "Implementation of electrical impedance tomography for analysis of building moisture conditions," *COMPEL-The international journal for computation and mathematics in electrical and electronic engineering*, vol. 37, no. 5, pp. 1837–1861, Oct. 2018, doi: 10.1108/COMPEL-01-2018-0034.
- [3] H. S. Tapp, A. J. Peyton, E. K. Kemsley, and R. H. Wilson, "Chemical engineering applications of electrical process tomography," *Sensors and Actuators B: Chemical*, vol. 92, no. 1–2, pp. 17–24, Jul. 2003, doi: 10.1016/S0925-4005(03)00126-6.
- [4] S. R. Atefi, F. Seoane, and K. Lindecrantz, "Electrical bioimpedance cerebral monitoring. Preliminary results from measurements on stroke patients electrical bioimpedance cerebral monitoring. Preliminary results from measurements on stroke patients," in *Annual International Conference of the IEEE Engineering in Medicine and Biology Society*, 2012, no. August, doi: 10.1109/EMBC.2012.6345887.
- [5] M. S. Campisi, C. Barbre, A. Chola, G. Cunningham, V. Woods, and J. Viventi, "Breast cancer detection using high-density flexible electrode arrays and electrical impedance tomography," in *2014 36th Annual International Conference of the IEEE Engineering in Medicine and Biology Society*, Aug. 2014, pp. 1131–1134, doi: 10.1109/EMBC.2014.6943794.
- [6] G. Y. Jang *et al.*, "Integrated EIT system for functional lung ventilation imaging," *BioMedical Engineering OnLine*, vol. 18, no. 1, Dec. 2019, doi: 10.1186/s12938-019-0701-y.
- [7] C. Putensen, B. Hentze, S. Muenster, and T. Muders, "Electrical impedance tomography for cardio-pulmonary monitoring," *Journal of Clinical Medicine*, vol. 8, no. 8, Aug. 2019, doi: 10.3390/jcm8081176.
- [8] G. Singh, S. Anand, B. Lall, A. Srivastava, and V. Singh, "Low-cost multifrequency electrical impedance-based system (MFEIBS) for clinical imaging: design and performance evaluation," *Journal of Medical Engineering and Technology*, vol. 42, no. 4, pp. 274–289, May 2018, doi: 10.1080/03091902.2018.1478008.
- [9] A. H. Al-Rawi, W. M. A. Ibrahim, and E. H. Mirza, "DC feedback for wide band frequency fixed current source," *Journal of Electrical Bioimpedance*, vol. 4, no. 1, pp. 33–37, Mar. 2013, doi: 10.5617/jeb.294.
- [10] A. B. S. Umbu and Endarko, "The design of voltage controlled current source (VCCS) for single frequency electrical impedance tomography (EIT)," in *2017 International Seminar on Sensors, Instrumentation, Measurement and Metrology (ISSIMM)*, Aug. 2017, pp. 30–36, doi: 10.1109/ISSIMM.2017.8124256.
- [11] M. Khalighi, B. V. Vahdat, M. Mortazavi, and M. Mikaeili, "Design and implementation of precise hardware for electrical impedance tomography (EIT)," *IJST, Transactions of Electrical Engineering*, vol. 38, pp. 1–20, 2014.
- [12] J. Huang, Y. Hung, J. Wang, and B. Lin, "Design of wearable and wireless electrical impedance tomography system," *Measurement*, vol. 78, pp. 9–17, Jan. 2016, doi: 10.1016/j.measurement.2015.09.031.
- [13] A. Widodo, "Design of low-cost and high-speed portable two-dimensional electrical impedance tomography (EIT)," *International Journal of Engineering and Technology*, vol. 7, no. 4, pp. 6458–6463, 2019, doi: 10.14419/ijet.v7i4.23298.
- [14] J. Wu, X. Chen, and Z. Ding, "Digital biomedical electrical impedance tomography based on FPGA," *Journal of Biosciences and Medicines*, vol. 1, no. 2, pp. 14–18, 2013, doi: 10.4236/jbm.2013.12004.
- [15] M. K. Choi, B. Harrach, and J. K. Seo, "Regularizing a linearized EIT reconstruction method using a sensitivity-based factorization method," *Inverse Problems in Science and Engineering*, vol. 22, no. 7, pp. 1029–1044, Oct. 2014, doi: 10.1080/17415977.2013.850682.
- [16] G. González, V. Kolehmainen, and A. Seppänen, "Isotropic and anisotropic total variation regularization in electrical impedance tomography," *Computers and Mathematics with Applications*, vol. 74, no. 3, pp. 564–576, 2017.
- [17] Y. Shi, Z. Rao, C. Wang, Y. Fan, X. Zhang, and M. Wang, "Total variation regularization based on iteratively reweighted least-squares method for electrical resistance tomography," *IEEE Transactions on Instrumentation and Measurement*, vol. 69, no. 6, pp. 3576–3586, Jun. 2020, doi: 10.1109/TIM.2019.2938640.
- [18] Y. Wang, "Anisotropic TV regularization in electrical impedance tomography: an experimental study," *Engineering*, vol. 14, no. 3, pp. 138–146, 2022, doi: 10.4236/eng.2022.143013.
- [19] T. Li, D. Isaacson, J. C. Newell, and G. J. Saulnier, "Adaptive techniques in electrical impedance tomography reconstruction," *Physiological Measurement*, vol. 35, no. 6, pp. 1111–1124, Jun. 2014, doi: 10.1088/0967-3334/35/6/1111.
- [20] Z. Wang, S. Yue, and X. Liu, "An iterative linear back-projection algorithm for electrical impedance tomography," in *2018 13th World Congress on Intelligent Control and Automation (WCICA)*, Jul. 2018, pp. 484–489, doi: 10.1109/WCICA.2018.8630576.
- [21] T. de C. Martins, M. de S. G. Tsuzuki, E. D. L. B. de Camargo, R. G. Lima, F. S. de Moura, and M. B. P. Amato, "Interval simulated annealing applied to electrical impedance tomography image reconstruction with fast objective function evaluation," *Computers and Mathematics with Applications*, vol. 72, no. 5, pp. 1230–1243, Sep. 2016, doi: 10.1016/j.camwa.2016.06.021.
- [22] R. S. Tavares, A. K. Sato, T. C. Martins, R. G. Lima, and M. S. G. Tsuzuki, "GPU acceleration of absolute EIT image reconstruction using simulated annealing," *Biomedical Signal Processing and Control*, vol. 52, pp. 445–455, Jul. 2019, doi: 10.1016/j.bspc.2017.02.007.
- [23] H. Kim, C. Boo, and M. Kang, "Image reconstruction using genetic algorithm in electrical impedance tomography," in *Neural Information Processing: 13th International Conference, ICONIP 2006, Hong Kong, China, October 3-6, 2006. Proceedings, Part III 13*, 2006, pp. 938–945.
- [24] S. J. Hamilton and A. Hauptmann, "Deep D-Bar: real-time electrical impedance tomography imaging with deep neural networks," *IEEE Transactions on Medical Imaging*, vol. 37, no. 10, pp. 2367–2377, Oct. 2018, doi: 10.1109/TMI.2018.2828303.
- [25] X. Li *et al.*, "A novel deep neural network method for electrical impedance tomography," *Transactions of the Institute of Measurement and Control*, vol. 41, no. 14, pp. 4035–4049, Oct. 2019, doi: 10.1177/0142331219845037.
- [26] D. Kang *et al.*, "Design 2-dimensional digital filter in reconstruction of EIT," in *ICCAS2004*, 2004, pp. 36–39.
- [27] B. Gong, B. Schullcke, S. Krueger-Ziolek, and K. Moeller, "Improving EIT image reconstruction with clustering," *IFAC-PapersOnLine*, vol. 48, no. 20, pp. 418–422, 2015, doi: 10.1016/j.ifacol.2015.10.176.
- [28] T. Li, T. J. Kao, D. Isaacson, J. C. Newell, and G. J. Saulnier, "Adaptive Kaczmarz method for image reconstruction in electrical impedance tomography," *Physiological Measurement*, vol. 34, no. 6, pp. 595–608, 2013, doi: 10.1088/0967-3334/34/6/595.
- [29] L. Zhang, "A modified Landweber iteration algorithm using updated sensitivity matrix for electrical impedance tomography," *International Journal of Advanced Pervasive and Ubiquitous Computing*, vol. 5, no. 1, pp. 17–29, 2013.





- [30] Q. Wang *et al.*, “An image reconstruction algorithm for electrical impedance tomography using Symkaczmarz based on structured sparse representation,” *Transactions of the Institute of Measurement and Control*, vol. 41, no. 10, pp. 2803–2815, Jun. 2019, doi: 10.1177/0142331218812563.
- [31] J. Wang and B. Han, “Application of a class of iterative algorithms and their accelerations to Jacobian-based linearized EIT image reconstruction,” *Inverse Problems in Science and Engineering*, vol. 29, no. 8, pp. 1108–1126, Aug. 2021, doi: 10.1080/17415977.2020.1826473.
- [32] H. Li and Z. Wan, “A modified algebraic reconstruction algorithm for sparse projection,” *Annals of Translational Medicine*, vol. 9, no. 18, pp. 1422–1422, Sep. 2021, doi: 10.21037/atm-21-3529.
- [33] K. Arya, Y. Pathak, and S. Tiwari, “Regularization based modified SART iterative method for CT image reconstruction,” in *2016 9th International Conference on Developments in eSystems Engineering (DeSE)*, 2019, pp. 217–222.
- [34] J. Liang, W. He, D. Ji, and L. Wang, “Image reconstruction algorithm for modified SART based on PM model,” in *2015 11th International Conference on Computational Intelligence and Security (CIS)*, Dec. 2015, no. 1, pp. 175–178, doi: 10.1109/CIS.2015.50.
- [35] A. Boudjelal, Z. Messali, A. Elmoataz, and B. Attallah, “Improved simultaneous algebraic reconstruction technique algorithm for positron-emission tomography image reconstruction via minimizing the fast total variation,” *Journal of Medical Imaging and Radiation Sciences*, vol. 48, no. 4, pp. 385–393, Dec. 2017, doi: 10.1016/j.jmir.2017.09.005.
- [36] T. Hobiger, T. Kondo, and Y. Koyama, “Constrained simultaneous algebraic reconstruction technique (C-SART) - a new and simple algorithm applied to ionospheric tomography,” *Earth, Planets and Space*, vol. 60, no. 7, pp. 727–735, Jul. 2008, doi: 10.1186/BF03352821.
- [37] R. Aprilliyani, R. G. Prabowo, and Basari, “On the performance of SART and ART algorithms for microwave imaging,” in *AIP Conference Proceedings*, 2018, vol. 1933, doi: 10.1063/1.5023980.
- [38] A. Adler and W. R. B. Lionheart, “Uses and abuses of EIDORS: an extensible software base for EIT,” *Physiological Measurement*, vol. 27, no. 5, pp. S25–S42, May 2006, doi: 10.1088/0967-3334/27/5/S03.
- [39] P. C. Hansen and J. S. Jørgensen, “AIR Tools II: algebraic iterative reconstruction methods, improved implementation,” *Numerical Algorithms*, vol. 79, no. 1, pp. 107–137, Sep. 2018, doi: 10.1007/s11075-017-0430-x.
- [40] B. Brown, “Electrical impedance tomography (EIT): a review,” *Journal of Medical Engineering and Technology*, vol. 27, no. 3, pp. 97–108, Jan. 2003, doi: 10.1080/0309190021000059687.
- [41] B. Zhao, H. Wang, X. Chen, X. Shi, and W. Yang, “Linearized solution to electrical impedance tomography based on the Schur conjugate gradient method,” *Measurement Science and Technology*, vol. 18, no. 11, pp. 3373–3383, Nov. 2007, doi: 10.1088/0957-0233/18/11/017.
- [42] D. Arthur and S. Vassilvitskii, “K-means ++: the advantages of careful seeding,” in *Proceedings of the Eighteenth Annual ACM-SIAM Symposium on Discrete Algorithms*, 2007, pp. 1027–1035, doi: 10.1145/1283383.1283494.
- [43] A. Widodo and Endarko, “Experimental study of one step linear Gauss-Newton algorithm for improving the quality of image reconstruction in high-speed electrical impedance tomography (EIT),” *Journal of Physics: Conference Series*, vol. 1120, no. 1, 2018, doi: 10.1088/1742-6596/1120/1/012067.
- [44] Q. Wang, F. Li, J. Wang, X. Duan, and X. Li, “Towards a combination of low rank and sparsity in EIT imaging,” *IEEE Access*, vol. 7, pp. 156054–156064, 2019, doi: 10.1109/ACCESS.2019.2947439.
- [45] Z. Wang, A. C. Bovik, H. R. Sheikh, and E. P. Simoncelli, “Image quality assessment: from error visibility to structural similarity,” *IEEE Transactions on Image Processing*, vol. 13, no. 4, pp. 600–612, Apr. 2004, doi: 10.1109/TIP.2003.819861.
- [46] J. Zhang *et al.*, “HF-SENSE: An improved partially parallel imaging using a high-pass filter,” *BMC Medical Imaging*, vol. 19, no. 1, pp. 1–10, 2019, doi: 10.1186/s12880-019-0327-3.

BIOGRAPHIES OF AUTHORS






Arfan Eko Fahrudin     received the Bachelor’s degree in Physics (2004) from Institut Teknologi Sepuluh Nopember (ITS) and a master’s degree in Electrical Engineering (2010) specializing in neural network and image processing from Universitas Gadjah Mada (UGM). He is currently reading for a doctorate at Institut Teknologi Sepuluh Nopember (ITS), Indonesia, funded by BPPDN Scholarships. His interdisciplinary research interests focus on biophysics, biomedical instrumentation, and image processing. He can be contacted at arfan_eko@ulm.ac.id.






Endarko     received the Bachelor’s degree in Electronics and Instrumentation (1998) from Universitas Gadjah Mada (UGM), a master’s degree in Physics (2003) specializing in instrumentation physics from Institut Teknologi Bandung (ITB), and a Ph.D. degree in Electronic and Electrical Engineering from University of Strathclyde, Glasgow, UK (2012). Since 1998, he has worked at the Department of Physics, Institut Teknologi Sepuluh Nopember (ITS) in Surabaya. His interdisciplinary research interests focus on biophysics, medical physics, and medical instrumentation. He can be contacted at email: endarko@physics.its.ac.id.



Khusnul Ain    received the Bachelor's degree in Physics (1995) from Universitas Gadjah Mada (UGM), a master's degree in Physics specializing in computational physics (2002) from Universitas Gadjah Mada (UGM), and a Ph.D. degree in Medical Physics from Institut Teknologi Bandung (ITB) (2014). Since 1997, he has been working at the Department of Physics, Universitas Airlangga, in Surabaya. His interdisciplinary research interests focus on medical physics and medical instrumentation. He can be contacted at k_ain@fst.unair.ac.id.



Agus Rubiyanto    received the Bachelor's degree in Physics (1988) from Institut Teknologi Sepuluh Nopember (ITS), a master's degree in Optoelectronics and Applied Laser (1993) from Universitas Indonesia, and a Ph.D. degree in Applied Physics from University of Paderborn, Germany (2000). Since 1989, he has worked at the Department of Physics, Institut Teknologi Sepuluh Nopember (ITS) in Surabaya. His interdisciplinary research interests focus on optoelectronics, medical physics, and biophysics. He can be contacted at email: arubi@physics.its.ac.id.